Article:
Thomas, SA, Mishra, B and Myneni, SCB (2019) High Energy Resolution-X-ray Absorption Near Edge Structure Spectroscopy Reveals Zn Ligation in Whole Cell Bacteria. Journal of Physical Chemistry Letters, 10. pp. 2585-2592. ISSN 1948-7185

https://doi.org/10.1021/acs.jpclett.9b01186

Spectroscopy and Photochemistry; General Theory

High Energy Resolution (HR)-XANES Spectroscopy Reveals Zn Ligation in Whole Cell Bacteria

Sara Anne Thomas, Bhoopesh Mishra, and Satish C.B. Myneni

J. Phys. Chem. Lett., **Just Accepted Manuscript** • DOI: 10.1021/acs.jpclett.9b01186 • Publication Date (Web): 30 Apr 2019

High Energy Resolution (HR)-XANES Spectroscopy Reveals Zn Ligation in Whole Cell Bacteria

Sara A. Thomas,[1]* Bhoopesh Mishra,[2] and Satish C. B. Myneni[1]*

[1] Department of Geosciences, Princeton University, Guyot Hall, Princeton, NJ, 08544
[2] School of Chemical and Process Engineering, University of Leeds, Leeds LS2 9JT, UK

* Corresponding authors:
Sara A. Thomas
Email: st18@princeton.edu
Phone: (609)-258-2339

Satish Myneni
Email: smyneni@princeton.edu
Phone: (609)-258-5848

Abstract

Identifying the zinc (Zn) ligation and coordination environment in complex biological and environmental systems is crucial to understand the role of Zn as a biologically essential but sometimes toxic metal. Most studies on Zn coordination in biological or environmental samples rely on the extended X-ray absorption fine structure (EXAFS) region of a Zn K-edge X-ray absorption spectroscopy (XAS) spectrum. However, EXAFS analysis cannot identify unique nearest neighbors with similar atomic number (i.e., O versus N) and provides little information on Zn ligation. Herein, we demonstrate that high energy-resolution X-ray absorption near edge structure (HR-XANES) spectroscopy enables the direct determination of Zn ligation in whole cell bacteria, providing additional insights lost from EXAFS analysis at a fraction of the scan time and Zn concentration. HR-XANES is a relatively new technique that has improved our understanding of trace metals (e.g., Hg, Cu, and Ce) in dilute systems. This study is the first to show that HR-XANES can unambiguously detect Zn coordination to carboxyl, phosphoryl, imidazole, and/or thiol moieties in model microorganisms.

TOC graphic

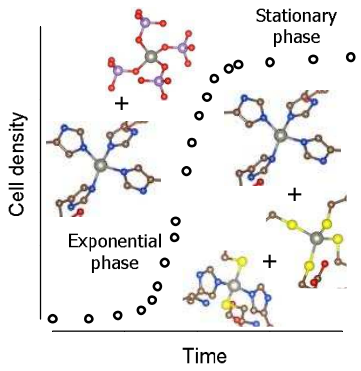

Zinc (Zn) is an essential metal for life in all organisms as it is a cofactor in various enzymes and plays an indispensable structural role in proteins.[1-3] However, due to its high stability relative to other essential, divalent transition metals,[4] Zn can displace vital metals from proteins and inhibit protein function above certain concentrations.[5] Within cells, Zn homeostasis is achieved via feedback mechanisms for import, shuttling to required sites, storage, and export.[6-9] To achieve the delicate balance between necessity and toxicity, Zn remains tightly bound within cells.[6] How Zn is coordinated intracellularly, at the cell surface, and in the extracellular milieu (i.e., the environment) determines its function and reactivity. Thus, understanding the role of Zn in biology requires detailed knowledge of Zn coordination in complex biological and environmental systems at relevant Zn concentrations (nM to mM).

Zn is considered borderline between a soft and hard Lewis acid and thus has an equal affinity for both O- and S-containing ligands.[10] The ability of Zn to be stable in many coordination environments creates multiple possibilities for Zn speciation in undefined samples. Previous studies on Zn(II) coordination in biological and environmental systems predominantly have relied on X-ray absorption spectroscopy (XAS), in particular the extended X-ray absorption fine structure (EXAFS) region, to obtain coordination information because the samples are not required to be crystalline. While EXAFS is successful in differentiating Zn bound to O/N versus S,[11] first shell analysis fails to identify Zn bound to O versus N (i.e., scattering shells that are indistinguishable in the EXAFS due to similar atomic number) as well as the nature of the coordinating ligand. Thiols are the likely identity of the S-containing moiety that binds Zn, but the O/N-containing moieties could be carboxyl, phosphoryl, imidazole (histidine), and/or amine. Also, the sample must be fairly concentrated (hundreds of ppm) in order to achieve a suitable EXAFS spectrum for analysis beyond the nearest neighbors. As a result, in-depth investigations into the nature of Zn-coordinating ligands are lacking, especially in complex, dilute systems.

In contrast, the X-ray absorption near edge structure (XANES) region of a XAS spectrum is sensitive to the nature of the coordinating ligand and other factors including the oxidation state and geometry of

the coordination polyhedron. In addition, XANES can be collected for samples with metal concentrations down to two orders of magnitude less than the levels examined by EXAFS.[12] However, due to the finite lifetime of the core hole generated during a XAS measurement, broadening of spectral features in the XANES can obscure the analysis. The recent development of high energy resolution (HR)-XANES to overcome the limitations of core-hole broadening[13] has led to advances in our understanding of metals at dilute concentrations (in some cases < 1 ppm) in complex biological and environmental systems including Hg,[14-18] Ce,[19] and Cu.[20] In addition, HR-XANES enhances sensitivity towards pre-edge features and structural distortion,[21-23] and the experimental setup also enables detailed X-ray emission spectroscopy.[24, 25] Herein, we present the first investigation into Zn speciation in biological systems with HR-XANES. We chose to probe a Gram-negative model bacterium (*Pseudomonas putida*) and a Gram-positive model bacterium (*Bacillus subtilis*) with HR-XANES as a function of growth stage and added Zn concentration to observe how these factors affect Zn coordination.

A comparison of Zn K-edge conventional and HR-XANES for biologically- and environmentally-relevant Zn compounds is presented in Figure 1. The Zn references include crystalline $Zn_3(PO_4)_2$ and $Zn(acetate)_2 \cdot 2H_2O$, which were chosen to represent Zn binding to the phosphoryl and carboxyl moieties, respectively, common in biological macromolecules (e.g., nucleic acid and proteins). In addition, we have included the HR-XANES of $ZnS_{(s)}$ (sphalerite) – a common environmental form of Zn. We also present HR-XANES of aqueous Zn complexes with low molecular weight ligands that represent Zn coordination to thiol (cysteine), imidazole (histidine), and carboxyl (malate) moieties – common Zn binding environments in proteins. HR- and conventional XANES spectra of additional Zn compounds are provided in Figure S1.

Zn is tetrahedrally and octahedrally coordinated to O atoms in $Zn_3(PO_4)_2$[26] and $Zn(acetate)_2 \cdot 2H_2O$,[27] respectively, while Zn is tetrahedrally coordinated to S atoms in $ZnS_{(s)}$.[28] The Zn coordination environment of the aqueous references was initially undefined and thus further assessed by EXAFS analysis (Figure S2 and Table S2). We confirmed that Zn is bound to 4 thiols from 4 cysteine molecules

(i.e., $Zn(cysteine)_4$) at a distance of 2.32 Å in the aqueous Zn-cysteine reference. In aqueous Zn-malate, Zn is bound to 6 O atoms at a distance of 2.05 Å, possibly from bidentate coordination from carboxyl and hydroxyl groups of 3 malate molecules (i.e., $Zn(malate)_3$), as reported in Zhang et al.[29] The EXAFS of the aqueous Zn-histidine reference fits well considering 4 N atoms bound to Zn at a distance of 2.03 Å as well as 8 C atoms from the imidazole rings at a radial distance of 3.01 Å, suggesting a $Zn(histidine)_{4(aq)}$ complex. We note that charges are not provided for the aqueous complexes shown in Figure 1 due to a lack of thermodynamic data for the presented structures.

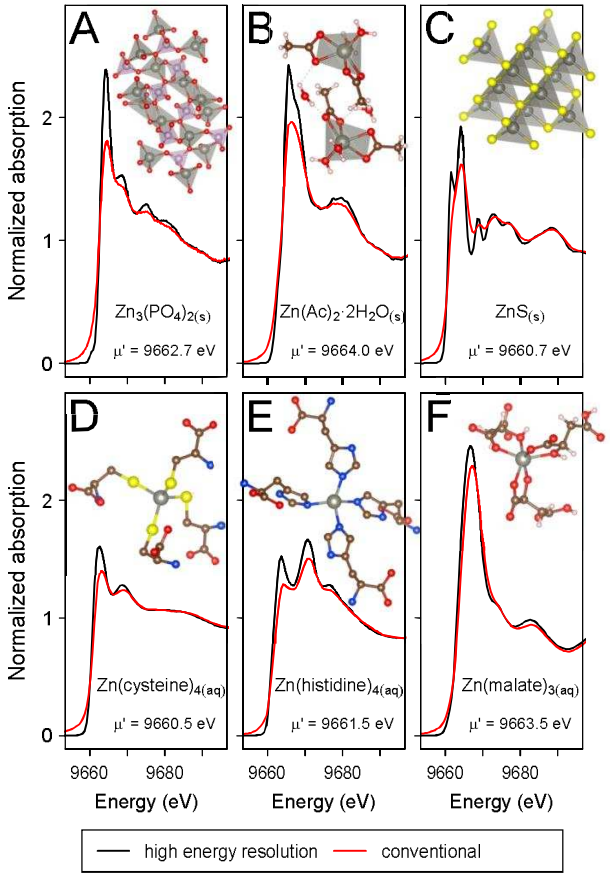

Figure 1. Zn K-edge XANES measured in conventional mode (transmission; red line) and high energy resolution (HR) mode (black line) of biologically- and environmentally-relevant Zn reference compounds. The crystalline references include (A) $Zn_3(PO_4)_2$,[26] (B) $Zn(acetate)_2 \cdot 2H_2O$,[27] and (C) ZnS.[28] The aqueous references include (D) $Zn(cysteine)_4$, (E) $Zn(histidine)_4$, and (F) $Zn(malate)_3$ and their presented local molecular structure was confirmed by EXAFS fitting (Supporting Information). The conventional and HR spectra were collected simultaneously and are overlaid to show the enhanced spectral features in the HR spectra. The edge position (μ′) of the HR-XANES is presented for each Zn compound.

The identity and number of the atoms in the first coordination shell for the Zn standards in Figure 1 is reflected in the edge position (μ′) and spectral features of the HR-XANES, which arise from Zn 1*s* to Zn 4*sp* or Zn 4*p* transitions as well as multiple scattering.[30] The energy of the absorption edge of a XANES spectrum is typically affected most dramatically by the oxidation state of the target element. However, at a fixed oxidation state, as is the case for Zn(II) in this study, the edge energy is also influenced by the electronegativity and number of coordinating atoms, bond angles, nearest-neighbor interatomic distances, and higher coordination spheres.[31] To gain an understanding of how different Zn coordination environments are reflected in the edge energy and XANES spectral features, we compared the intensity of the strongest electronic transition with the absorption edge energy of HR-XANES (Figure 2A) as well as conventional XANES (Figure 2B) spectra for various Zn references. The intensity of the strongest electronic transition is defined as the maximum absorption height in the XANES spectrum, and the absorption edge energy is defined as the energy at one half the maximum absorption height. There is a clear separation between the Zn species that are bound to S/N atoms and the Zn species that are bound to O atoms in both the HR- and conventional XANES (Figure 2). ZnS and Zn(cysteine)$_4$ have the lowest edge energies likely because the nearest neighbor for both (S) is the least electronegative out of O, N, and S. Zn(histidine)$_4$ and Zn-phthalocyanine – tetrahedral (Td) and square planar Zn-N species, respectively – have slightly greater edge energies than the Zn-S species. O is the most electronegative Zn-coordinating atom, which explains why the Zn-O species all have the highest edge energies, with octahedral (Oh) Zn-O species having higher absorption edge energies than Td Zn-O species.[32] In addition, Oh Zn-O species have characteristically high maximum absorption intensities,[32, 33] followed by Td Zn-O, and then the Zn-S and Zn-N species.

Figure 2 shows the wide variety of edge energies and maximum absorption intensities that can exist for pure Zn(II) species and can be useful when selecting standards to determine Zn ligation by HR-XANES linear combination fitting (LCF). Most notably, the references of Zn predominantly bound to O

versus S/N are distinct for both Figure 2A and 2B. However, it is important to note that normalization and energy calibration of XANES spectra as well as structural distortion can influence these features. Thus, the data presented in Figure 2 were carefully aligned in energy and normalized. In addition, the existence of multiple Zn coordination environments in a sample causes an averaging effect for both energy and intensity of the resulting XANES spectrum, which limits our ability to associate edge energy/maximum absorption intensity with certain Zn coordination environments. This is demonstrated with the Zn-O standards with mixed Oh and Td coordination in Figure 2B (i.e., hydrozincite – $Zn_5(CO_3)_2(OH)_6$ – and hopeite – $Zn_3(PO_4)_2 \cdot 4H_2O$), which have the lowest maximum absorption intensities among the Zn-O standards but remain unique from Zn-S/N due to their higher edge energy. Differences in coordination geometry when Zn is bound to the same ligands can also affect the XANES absorption edge energy, although Waychunas et al. report the effect is small.[32]

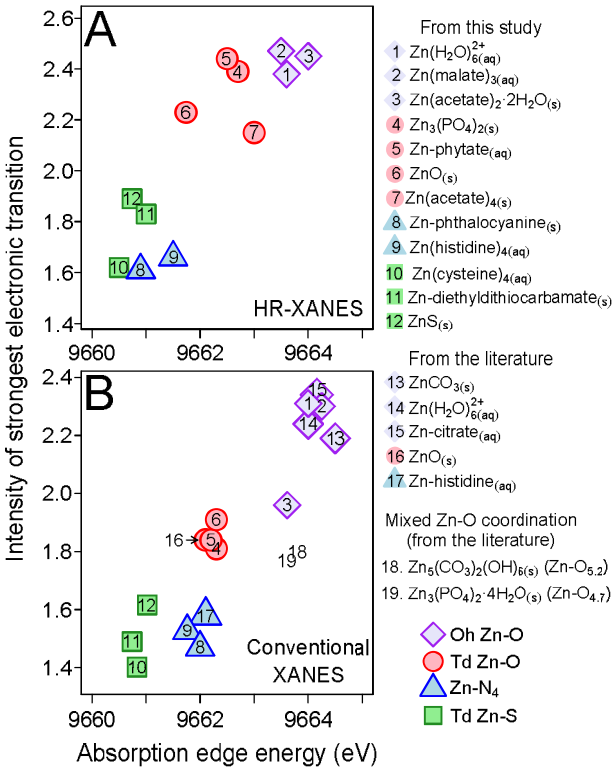

Figure 2. The intensity of the strongest electronic transition plotted against the absorption edge energy obtained from the (A) HR- and (B) conventional XANES spectra of Zn reference compounds (Figure 1 or Figure S1) with octahedral (Oh), tetrahedral (Td), and square planar Zn coordination environments. The intensity of the strongest electronic transition (Zn 1*s* to 4*sp* or 4*p*) was taken as the most intense

absorption peak in the XANES and the absorption edge energy was defined as the energy at one half the maximum absorption. (B) Additional references from Salt et al. (14 and 16) and Tang et al. (12, 13, 15, 17, and 18) that were normalized and aligned in energy with our spectra were included.[34, 35]

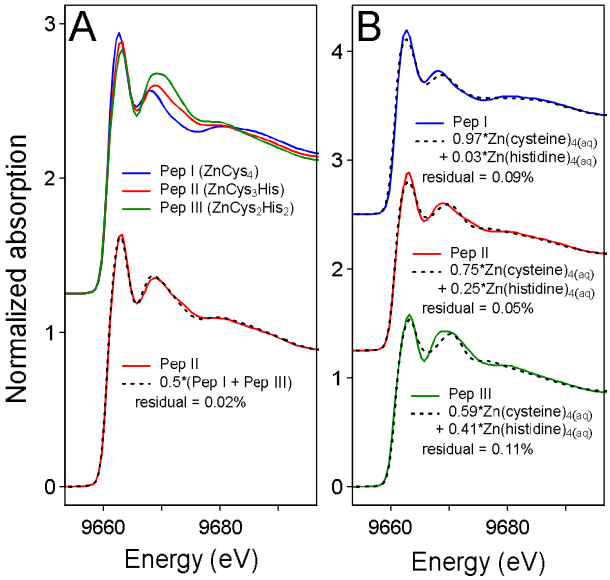

Figure 3. Zn K-edge HR-XANES of (A) Zn bound to peptides with Cys_4 (Pep I), Cys_3His (Pep II), and Cys_2His_2 (Pep III) coordination. (B) Best-fit LCF results to the HR-XANES of Zn-peptides using $Zn(cysteine)_4$, and $Zn(histidine)_4$ as standards provide (within 10%) the Zn ligation in the Zn-peptides. Residual = $\left[\sum_{i=1}^{N}(x_{data}(i) - x_{fit}(i))^2 / \sum_{i=1}^{N}(x_{data}(i))^2\right] \times 100\%$.

Clearly the conventional XANES can provide useful information (Figure 2). However, when identifying Zn ligation by LCF, the enhanced spectral features of HR-XANES provide a statistical advantage over conventional XANES (Figure S3,S4). Because Zn-N and Zn-S species overlap in Figure 2, we show that LCFs to the HR-XANES with $Zn(cysteine)_4$ and $Zn(histidine)_4$ as references can identify (within 10%) the Zn ligation in peptides with $ZnCys_4$ (Pep I), $ZnCys_3His$ (Pep II), and $ZnCys_2His_2$ (Pep III) coordination (Figure 3). The Zn coordination in the peptides is well-characterized[11, 36, 37] and represents common Zn binding environments in Zn finger proteins, which are characteristically small proteins that require Zn to stabilize the fold. We confirmed the expected Zn binding environment in the Zn-peptide samples with EXAFS fitting (Figure S2 and Table S2). The slight differences between the LCF spectra and the Zn-peptide spectra are likely due to geometrical differences in Zn-ligand coordination, which is particularly visible in the XANES region due to the prominence of multiple scattering effects.[38] However, as we demonstrate with the

peptide example in Figure 3, LCFs to the HR-XANES can still identify Zn ligation within reasonable accuracy when the Zn-ligand coordination geometry is unknown. Understanding the effect of coordination geometry on the spectral features of Zn K-edge HR-XANES would be a topic for future studies to potentially gain more information on Zn bonding beyond the identity of the ligands.

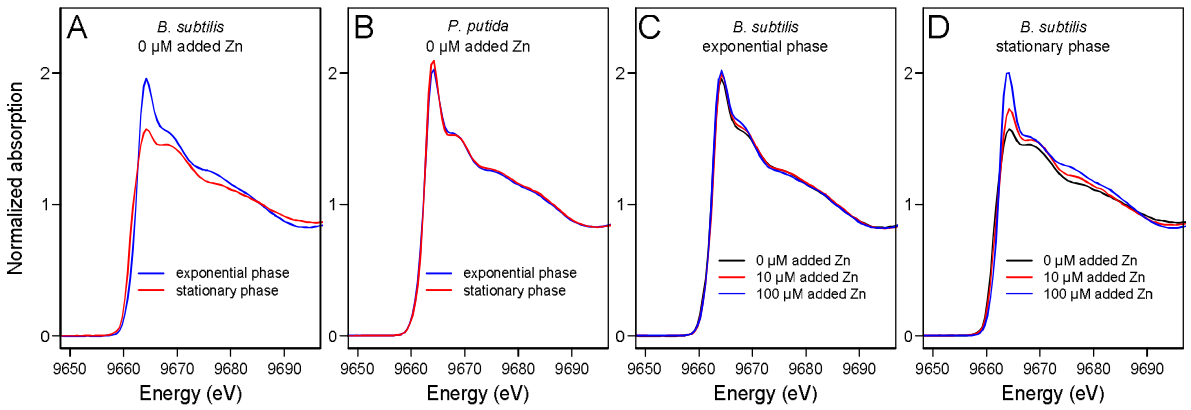

Figure 4. Zn K-edge HR-XANES of (A) *B. subtilis* and (B) *P. putida* with no additional added Zn that were harvested in exponential and stationary growth phase as well as *B. subtilis* in (C) exponential growth phase and (D) stationary growth phase exposed to 0, 10, and 100 µM Zn as $Zn(NO_3)_{2(aq)}$ for 2 hours. The Zn exposure medium was identical for both growth phases; however, the stationary phase medium did not contain glucose.

Zn K-edge HR-XANES spectra of *B. subtilis* and *P. putida* samples harvested in exponential and stationary growth phase, adjusted to OD_{600} ~ 0.2 (0.3 – 0.4 g per L, wet weight), and exposed to 0 – 100 µM of additional Zn for 2 hours are provided in Figure 4. A comparison of the HR-XANES spectra of cells harvested in exponential versus stationary phase reveals variations in the Zn coordination environment for *B. subtilis* (Figure 4A) but nearly identical Zn coordination environments for *P. putida* (Figure 4B). Zn in these bacterial samples came from the growth media, which contained 2.4 µM and 3.8 µM Zn for *B. subtilis* and *P. putida*, respectively. Due to similar amounts of Zn in the growth media, the differences observed for the 2 bacterial species at exponential and stationary growth stages likely reflect differences in the utilization and localization of Zn. We also explored the effect of Zn exposure on the Zn coordination environment in *B. subtilis*. From the HR-XANES, it is clear that Zn addition to exponential phase *B. subtilis*

had no effect on Zn coordination (Figure 4C), while the Zn addition did have an effect on Zn coordination in stationary phase cells (Figure 4D).

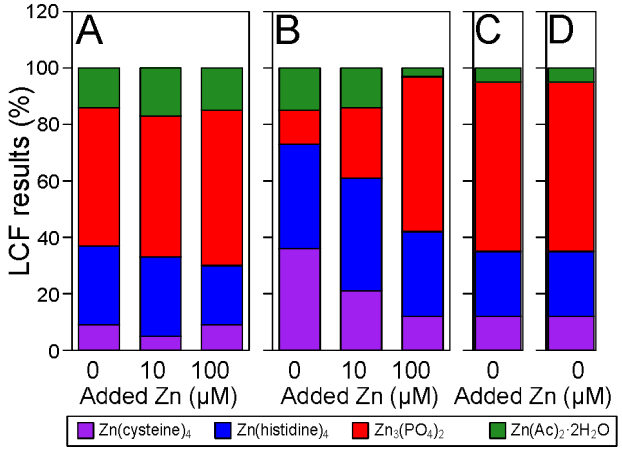

Figure 5. The LCF results (%) for (A) *B. subtilis* in exponential phase, (B) *B. subtilis* in stationary phase, (C) *P. putida* in exponential phase, and (D) *P. putida* in stationary phase exposed to 0 – 100 μM Zn using $Zn(cysteine)_4$, $Zn(histidine)_4$, $Zn_3(PO_4)_2$, and $Zn(acetate)_2 \cdot 2H_2O$ as standards. LCF results of other fit models are included in Table S3. The standard error is < 4% for each sample.

To obtain quantitative Zn coordination environment information for the bacterial samples, we performed LCFs of the HR-XANES using Zn standards to represent 4 functional groups in bacteria capable of binding Zn – i.e., phosphoryl, carboxyl, imidazole, and thiol (Figures 5, Figure S6). Among the six fit models we tested (Table S3, Figure S5), the $Zn_3(PO_4)_2$, $Zn(acetate)_2 \cdot 2H_2O$, $Zn(histidine)_4$, and $Zn(cysteine)_4$ references were necessary for a good fit. The *B. subtilis* sample harvested in stationary phase and exposed to 0 μM added Zn contains the highest fraction of Zn bound to cysteine and histidine (Figure 5). The addition of 10 μM Zn to the stationary phase cells decreases the fraction of Zn-cysteine coordination while Zn-histidine coordination remains unchanged (Figure 5). Increasing added Zn to 100 μM for stationary phase *B. subtilis* further decreases the Zn-cysteine coordination as well as the Zn-histidine coordination. The remainder of the Zn speciation is made up of a majority of $Zn_3(PO_3)_2$ and a low fraction of $Zn(acetate)_2 \cdot 2H_2O$. There are small differences among the Zn coordination results of the *B. subtilis* samples in exponential growth phase exposed to 0 – 100 μM Zn as well as the *P. putida* samples in both exponential

and stationary growth phase, which resemble the results of the *B. subtilis* sample in stationary growth phase exposed to 100 µM Zn (Figure 5).

We also performed EXAFS analyses on the bacterial samples by non-linear least squares fitting of the EXAFS equation (Table 1, Figure S7). For all *B. subtilis* samples in exponential growth phase, the *B. subtilis* sample in stationary phase that was exposed to 100 µM Zn, and all *P. putida* samples in exponential and stationary growth phase, the EXAFS fit well considering that Zn is coordinated to 4 O/N atoms. Due to the low signal to noise ratio in the EXAFS of the bacterial samples and short k range (2 – 11 $Å^{-1}$), we did not perform second shell EXAFS fitting. The only samples that require the inclusion of a Zn-S shell are *B. subtilis* in stationary phase exposed to 0 µM and 10 µM of additional Zn (Table 1). The EXAFS fit results show that Zn-S coordination accounts for 47 ± 10% and 22 ± 7% of the total cell-associated Zn, respectively, which agrees with the HR-XANES LCF results. However, the knowledge of Zn binding specifically to phosphoryl, carboxyl, and imidazole groups in the bacterial samples is lost in the EXAFS analysis.

Table 1: EXAFS structural fit parameters for bacterial samples containing Zn[a,b,c,d,e]

B. subtilis	Added Zn (µM)	Shell	N	R (Å)	σ^2 ($\times 10^3$ $Å^2$)
	0	Zn-O/N[f]	3.77 ± 0.24	1.97 ± 0.01	5.03 ± 0.57
Exponential phase	10	Zn-O/N	3.88 ± 0.26	1.97 ± 0.01	5.03 ± 0.57
	100	Zn-O/N	3.78 ± 0.23	1.97 ± 0.01	5.03 ± 0.57
	0	Zn-O/N	1.98 ± 0.28	1.97 ± 0.01	2.51 ± 0.29
		Zn-S	1.75 ± 0.36	2.33 ± 0.03	7.54 ± 0.86
Stationary phase	10	Zn-O/N	2.99 ± 0.27	1.97 ± 0.01	5.03 ± 0.57
		Zn-S	0.82 ± 0.27	2.34 ± 0.02	7.54 ± 0.86
	100	Zn-O/N	3.96 ± 0.22	1.97 ± 0.01	5.03 ± 0.57
P. putida					
Exponential phase	0	Zn-O/N	3.84 ± 0.22	1.97 ± 0.01	5.03 ± 0.57
Stationary phase	0	Zn-O/N	3.98 ± 0.20	1.97 ± 0.01	5.03 ± 0.57

[a] S_0^2 is fixed at 0.95 for all fits. [b] The 8 datasets were fit simultaneously with 23 variables and 38.8 independent points. [c] All fits had a k range of 2.0-10.2 $Å^{-1}$ and an R range of 1.1 – 2.0 Å, except stationary phase *B. subtilis* exposed to 0 µM and 10 µM Zn which had an R range of 1.1 – 2.25 Å and 1.1 – 2.20 Å, respectively. [d] All datasets shared an ΔE_0 variable which fit to -0.05 ± 0.36 eV. [e] Results of the fit are presented in Figure S7. [f] A Zn-N shell is indistinguishable from Zn-O in the EXAFS.

Because EXAFS spectra mainly depend on the radial distance of neighboring atoms from the absorbing atom, unique chemical species can have identical EXAFS. The ambiguity that can exist in EXAFS analysis is particularly a problem for Zn due to the complexity of Zn binding environments that can arise in biological and environmental systems. Many previous studies identified whether Zn was bound to O/N vs. S with EXAFS but could not provide the ligand identity.[39-42] With HR-XANES, we notably observe Zn binding to histidine in both *B. subtilis* and *P. putida*, which to our knowledge, has yet to be directly observed in whole cell bacterial samples. Although Zn binding to histidine residues is common in proteins (known from X-ray crystallography),[43] the inability to distinguish N from O binding with EXAFS has likely prevented the identification of Zn-histidine coordination in systems with multiple Zn sites. In addition, studies have typically assumed that Zn-N binding will not occur at neutral pH because amines are protonated at neutral pH and thus cannot bind Zn.[39, 41, 44] Interestingly, stationary phase *B. subtilis* exposed to no additional Zn contained the highest percentages of Zn-histidine and Zn-cysteine coordination. *B. subtilis* is known to form spores under conditions of environmental stress (e.g., the nutrient limited conditions characteristic of stationary growth phase),[45] which may be responsible for the different Zn coordination environments. In addition, the fact that the percentage of cysteine and histidine binding is similar in the stationary phase *B. subtilis* sample with no added Zn implies $ZnCys_2His_2$ coordination. Zn finger proteins commonly contain $ZnCys_2His_2$ binding sites and are involved in regulating cell death (apoptosis), which is expected for cells in stationary growth phase.[46] In contrast, the Zn coordination environment in *P. putida* exposed to no additional Zn did not change with growth phase. The unaffected Zn coordination environment could reflect a Zn usage or storage mechanism that differs from *B. subtilis* under nutrient limited conditions. It is also possible that a majority of the Zn that is associated with *P. putida* remains at the cell surface, where it presumably would not be affected by changes in growth stage.

We observed a predominance of Zn-phosphoryl binding in many bacterial samples, although we consciously excluded PO_4^{3-} from the exposure media due to the low solubility of $Zn_3(PO_4)_{2(s)}$. The

organophosphate (β-glycerophosphate, also known as glycerol 2-phosphate) in the exposure medium (1 mM) is known to weakly bind metals (logK of Zn-β-glycerophosphate = 2.1) and is not likely the phosphoryl source.[47] In addition, the *P. putida* samples and *B. subtilis* exponential phase sample that obtained all their Zn from the growth medium (0 μM added Zn) all exhibit > 50% Zn-phosphoryl binding, which should not be attributed to the β-glycerophosphate in the exposure medium. The bacterial cells may retain some inorganic PO_4^{3-} from the growth medium even after washing with the exposure medium which could react with the added Zn in the assay medium. However, other phosphoryl sources exist in bacteria that could bind Zn including macromolecules (e.g., nucleic acid),[39] phospholipids,[48] and even ATP.[10, 49] The abundance of phospholipids in the cell envelope could explain the increased Zn-phosphoryl binding with added Zn concentration in stationary phase *B. subtilis* as stationary phase cells are not expected to actively import Zn. In addition, we are not the first to report Zn binding to phosphoryl groups in microbial systems. Using knowledge from first and second shell EXAFS fitting, Sarret et al. reported Zn binding to phosphoryl groups in the isolated cell walls of *Penicillium chrysogenum* and only Zn binding to carboxyl groups after the phosphoryl groups were saturated with Zn.[41] In addition, Ha et al. employed EXAFS to report Zn(II) binding to O in the extracellular polymeric substance (EPS) layer and membrane of *Shewanella oneidensis*, and they inferred that Zn(II) was binding to phosphoryl groups with knowledge from potentiometric titrations.[44] Toner et al. also observed Zn(II) binding to predominantly phosphoryl groups in a bacterial biofilm.[50]

The intracellular free ion concentration of Zn is very low (i.e., nano- to femtomolar range),[6] and it is generally believed that the majority of cellular Zn is tightly bound to metalloproteins to avoid displacing other metals from their intended sites.[6, 51] However, the chemical speciation of the intracellular Zn pool is not well defined.[52] Our finding that Zn can bind predominantly to phosphoryl groups associated with bacterial cells suggests that, at the Zn concentrations in this study, the coordination chemistry of Zn is not dominated by binding sites in proteins because amino acid residues do not contain phosphoryl groups.

Potentially, a large fraction of Zn can occupy sites in the cell envelope in addition to being sequestered intracellularly by metalloproteins. Bacterial phosphoryl groups may be a sink for Zn in natural environments impacted by high Zn concentrations.

We have demonstrated that HR-XANES spectroscopy can be employed to obtain quantitative information on Zn ligation in complex biological systems using the spectral features of structurally well characterized model complexes. In contrast, first-shell EXAFS spectroscopy fails to identify the nature of the Zn-coordinating ligand, especially when Zn is bound to carboxyl, phosphoryl, and imidazole groups. For the first time using only XAS techniques, we show that the Zn coordination environment in 2 bacterial species involves a mixture of Zn-phosphoryl, Zn-carboxyl, Zn-thiol, and Zn-imidazole binding. Changes in growth phase affect Zn coordination in *B. subtilis* but not in *P. putida*. Our findings can be used to interpret how bacteria react to (in terms of uptake and storage) nutrient limitation and Zn exposure at short time scales. Future studies on the effect of coordination geometry and higher coordination spheres on the Zn K-edge HR-XANES will improve our ability to characterize Zn coordination in complex biological and environmental systems.

Experimental Methods

Bacterial species and exposure media. *Bacillus subtilis* 168 and *Pseudomonas putida* ATCC® 33015™ were generously donated by Jeremy Fein, University of Notre Dame and stored at -80 °C in glycerol stock. *B. subtilis* and *P. putida* were streaked from frozen stock onto individual LB agar plates, incubated for ~24 hours at room temperature, and stored at 4 °C in the refrigerator for no more than 1 month. A single colony of *B. subtilis* or *P. putida* was inoculated into nutrient sporulation medium phosphate[53] (NSMP) or modified M9 medium (Table S1), respectively, and shaken overnight at 150 rpm at room temperature (24 – 26 °C). *B. subtilis* and *P. putida* were harvested in both exponential and > 12 hours into stationary growth phase, washed twice (3,300 g for 10 minutes), and resuspended in the final exposure medium. The exposure medium for *B. subtilis* was modified from NSMP, eliminating undefined components and

phosphate, and contained 20 mM MOPS buffer, 1 mM Na-β-glycerophosphate, 0.13 mM methionine, 0.12 mM tryptophan, 10 mM glucose, 0.5% (v/v) metal mixture (140 mM $CaCl_2$, 10 mM $MnCl_2$, and 200 mM $MgCl_2$), and 5.0 mM NaOH (pH = 6.8). The exposure medium for *P. putida* contained 20 mM MOPS buffer, 1 mM Na-β-glycerophosphate, 0.1 mM NH_4Cl, 0.8 mM $MgSO_4 \cdot 7H_2O$, 10 mM glucose, and 7.5 mM NaOH (pH = 7.0). Glucose was eliminated from the exposure medium for cells harvested in stationary phase to further limit metabolic activity. For consistency, the final cell densities of exponential and stationary phase cells were kept at an OD_{600} of 0.2.

Zn(II) exposure assays. A 10 mM $Zn(NO_3)_2$ stock solution (trace metal grade) was used for all exposure assays and stored at 4 °C. Stock solutions were prepared in Milli-Q water at 20 times the final desired Zn(II) concentration immediately before addition to bacterial cell suspensions. The final Zn(II) concentrations included 0 µM, 10 µM, and 100 µM added Zn(II) for *B. subtilis* and 0 µM added Zn(II) for *P. putida*. The Zn(II) exposure assays were initiated by the addition of 2.5 mL of 20 times concentrated Zn(II) stock solution to 47.5 mL of exponential and stationary growth phase cell suspension in the respective exposure media. The assays were conducted in the dark in acid-washed 125 mL Erlenmeyer flasks sealed with foil. Cells were shaken at 150 rpm for 2 hours after which the solution was used for the determination of cell-associated Zn(II) speciation by HR-XANES (see below).

Preparation of bacterial samples, peptides, and references for XAS. After the 2 hour Zn(II) exposure period, the cells were washed twice with 0.1 M $NaClO_4$. After the final wash, the cell pellet was suspended in 500 µL of 0.1 M $NaClO_4$ and pipetted into a 1.5 mL microfuge tube fitted with an EMD Millipore centrifugal filter unit (Mfr # UFC510024). The filter provided in the unit was switched out for a 0.2 µm cellulose acetate filter (Whatman) that was cut with a ~7 mm diameter hole punch. The cell suspension was then centrifuged at 10,000g for 8 minutes, collecting the cell pellet on the filter. The pellet on the filter was then sandwiched between pieces of Kapton tape, plunged in LN_2, and kept frozen until analysis. The samples were shipped to the ESRF on dry ice (< 48 hours in transit).

The peptides with sequences ProTyrLysCys$_4$ProGluCys$_7$GlyLysSerPheSerGlnLysSerAspLeuValLysXaa$_{20}$GlnArgThrYaa$_{24}$ThrGly, where the metal coordination sites are Cys$_2$His$_2$ (Xaa = Yaa = His), Cys$_3$His (Xaa = His, Yaa = Cys), and Cys$_4$ (Xaa = Yaa = Cys), were purchased from Life Technologies Corporation (Carlsbad, CA) and prepared as previously described.[11] Specifically, a 10 mM peptide and 9 mM $Zn(NO_3)_2$ solution were prepared in 100 mM HEPES, 50 mM NaCl, pH = 7.0 buffer and allowed to equilibrate for 1 hour. Aqueous Zn-malate, Zn-histidine, and Zn-cysteine references (pH adjusted to 7.0 with NaOH) were prepared in Milli-Q water at a final $Zn(NO_3)_2$ concentration of 25 mM and a final ligand concentration of 250 mM. All liquid references were pipetted into copper sample holders and immediately flash frozen into LN_2 prior to HR-XANES measurement.

$Zn(acetate)_2 \cdot 2H_2O$, ZnS, and $Zn_3(PO_4)_2$ powders were purchased from Sigma Aldrich. The spectra collected of Zn-acetate, $Zn_3(PO_4)_2$, and Zn-phytate (pH = 7) were provided graciously by Emmanuel Doelsch and preparation details have been reported previously.[54] Zn powdered references were diluted to 0.1 – 0.4 wt% with boron nitride and pressed into 5 mm diameter pellets.

Collection and analysis of XAS spectra. Zn K-edge conventional XANES, HR-XANES, and EXAFS spectra were collected on the CRG-FAME-UHD beamline (BM16) at the European Synchrotron Radiation Facility (ESRF). The beamline is equipped with 2 Si(220) monochromators ($\Delta E/E = 5.6 \times 10^{-5}$). All samples were measured at ~10 K in high energy resolution fluorescence detection (HERFD) mode with 5 spherically bent Si crystal analyzers (bending radius = 1 m, crystal diameter = 0.1 m). The Zn $K_{\alpha 1}$ fluorescence line (8.638 keV) was selected using the 642 reflection, and the diffracted fluorescence was measured with a silicon drift detector (SDD, Vortex EX-90). The beam (size = 100 µm x 200 µm) was moved to a new position on the sample after each scan, and beam damage was not observed. The effective energy resolution in high resolution mode was calculated as 0.63 eV. The energy calibration was carefully maintained with a Zn foil placed behind the sample. Transmission data was also collected for Zn references that were of high enough concentration in order to obtain conventional XANES for comparison with HR-XANES. Data

normalization and processing were performed with Athena, R, and Larch.[55] Self-absorption was not an issue for the Zn references (0.1 – 0.4 wt %) or the bacterial samples (0.02 – 0.4 wt % Zn).

Quantification of total Zn. The concentration of total Zn in the growth media was measured on an ICap-Q single collector ICP-MS using NIST 1643f as an external standard and 500 ppb Sc as an internal standard.

Supporting Information

Growth media composition, HR-XANES of additional Zn references, EXAFS fit results of Zn references, statistical comparison of HR- vs. conventional XANES, comparison of LCF models to bacteria HR-XANES, difference spectra of HR-XANES and best-fit LCFs, plot of best-fit LCF for bacteria HR-XANES, non-linear least squares fits to bacteria EXAFS (PDF).

Author information

The authors declare no competing financial interests.

Acknowledgements

This work is supported by the National Science Foundation under grant EAR-1424899. The experiments were performed on beamline BM16 – UHD-FAME – at the European Synchrotron Radiation Facility (ESRF), Grenoble, France. The FAME-UHD project is financially supported by the French "grand emprunt" EquipEx (EcoX, ANR-10-EQPX-27-01), the CEA-CNRS CRG consortium, and the INSU CNRS institute. We are grateful for the beamline assistance of Dr. Olivier Proux at BM16. We also thank Professor Jeremy Fein for donating the bacterial strains in this study as well as Dr. Emmanuel Doelsch for providing the XANES spectra of $Zn_3(PO_4)_2$, $Zn(acetate)_2 \cdot 2H_2O$, and Zn-phytate. We appreciate the assistance of Nicolas Slater with the ICP-MS measurements.

References

1. Choi, S. Y.; Bird, A. J., Zinc'ing sensibly: controlling zinc homeostasis at the transcriptional level. *Metallomics* **2014,** *6* (7), 1198-1215.
2. Asmuss, M.; Mullenders, L. H. F.; Hartwig, A., Interference by toxic metal compounds with isolated zinc finger DNA repair proteins. *Toxicol. Lett.* **2000,** *112*, 227-231.
3. Berg, J. M.; Shi, Y. G., The galvanization of biology: A growing appreciation for the roles of zinc. *Science* **1996,** *271* (5252), 1081-1085.
4. Waldron, K. J.; Robinson, N. J., How do bacterial cells ensure that metalloproteins get the correct metal? *Nat. Rev. Microbiol.* **2009,** *7* (1), 25-35.
5. Hantke, K., Bacterial zinc uptake and regulators. *Curr. Opin. Microbiol.* **2005,** *8* (2), 196-202.
6. Outten, C. E.; O'Halloran, T. V., Femtomolar sensitivity of metalloregulatory proteins controlling zinc homeostasis. *Science* **2001,** *292* (5526), 2488-2492.
7. Colvin, R. A.; Holmes, W. R.; Fontaine, C. P.; Maret, W., Cytosolic zinc buffering and muffling: Their role in intracellular zinc homeostasis. *Metallomics* **2010,** *2* (5), 306-317.
8. Kambe, T.; Tsuji, T.; Hashimoto, A.; Itsumura, N., The physiological, biochemical, and molecular roles of zinc transporters in zinc homeostasis and metabolism. *Physiol. Rev.* **2015,** *95* (3), 749-784.
9. Maret, W.; Li, Y., Coordination Dynamics of Zinc in Proteins. *Chem. Rev.* **2009,** *109* (10), 4682-4707.
10. Krezel, A.; Maret, W., The biological inorganic chemistry of zinc ions. *Arch. Biochem. Biophys.* **2016,** *611*, 3-19.
11. Clark-Baldwin, K.; Tierney, D. L.; Govindaswamy, N.; Gruff, E. S.; Kim, C.; Berg, J.; Koch, S. A.; Penner-Hahn, J. E., The limitations of X-ray absorption spectroscopy for determining the structure of zinc sites in proteins. When is a tetrathiolate not a tetrathiolate? *J. Am. Chem. Soc.* **1998,** *120* (33), 8401-8409.
12. Heald, S. M., Strategies and limitations for fluorescence detection of XAFS at high flux beamlines. *J. Synchrotron Radiat.* **2015,** *22*, 436-445.
13. Proux, O.; Lahera, E.; Del Net, W.; Kieffer, I.; Rovezzi, M.; Testemale, D.; Irar, M.; Thomas, S.; Aguilar-Tapia, A.; Bazarkina, E. F.; Prat, A.; Tella, M.; Auffan, M.; Rose, J.; Hazemann, J.-L., High-energy resolution fluorescence detected X-ray absorption spectroscopy: A powerful new structural tool in environmental biogeochemistry sciences. *J. Environ. Qual.* **2017**.
14. Manceau, A.; Wang, J. X.; Rovezzi, M.; Glatzel, P.; Feng, X. B., Biogenesis of mercury-sulfur nanoparticles in plant leaves from atmospheric gaseous mercury. *Environ. Sci. Technol.* **2018,** *52* (7), 3935-3948.
15. Manceau, A.; Enescu, M.; Simionovici, A.; Lanson, M.; Gonzalez-Rey, M.; Rovezzi, M.; Tucoulou, R.; Glatzel, P.; Nagy, K. L.; Bourdineaud, J. P., Chemical forms of mercury in human hair reveal sources of exposure. *Environ. Sci. Technol.* **2016,** *50* (19), 10721-10729.
16. Manceau, A.; Lemouchi, C.; Enescu, M.; Gaillot, A. C.; Lanson, M.; Magnin, V.; Glatzel, P.; Poulin, B. A.; Ryan, J. N.; Aiken, G. R.; Gautier-Luneau, I.; Nagy, K. L., Formation of mercury sulfide from Hg(II)-thiolate complexes in natural organic matter. *Environ. Sci. Technol.* **2015,** *49* (16), 9787-9796.
17. Manceau, A.; Bustamante, P.; Haouz, A.; Bourdineaud, J. P.; Gonzalez-Rey, M.; Lemouchi, C.; Gautier-Luneau, I.; Geertsen, V.; Barruet, E.; Rovezzi, M.; Glatzel, P.; Pin, S., Frontispiece: Mercury(II) binding to metallothionein in *Mytilus edulis* revealed by high energy-resolution XANES spectroscopy. *Chem.: Eur. J.* **2019,** *25* (4).
18. Bourdineaud, J.-P.; Gonzalez-Rey, M.; Rovezzi, M.; Glatzel, P.; Nagy, K. L.; Manceau, A., Divalent mercury in dissolved organic matter is bioavailable to fish and accumulates as dithiolate and tetrathiolate complexes. *Environ. Sci. Technol.* **2019**. DOI: 10.1021/acs.est.8b06579

19. Tella, M.; Auffan, M.; Brousset, L.; Morel, E.; Proux, O.; Chaneac, C.; Angeletti, B.; Pailles, C.; Artells, E.; Santaella, C.; Rose, J.; Thiery, A.; Bottero, J. Y., Chronic dosing of a simulated pond ecosystem in indoor aquatic mesocosms: Fate and transport of CeO_2 nanoparticles. *Environ. Sci.-Nano* **2015,** *2* (6), 653-663.
20. De Santis, E.; Shardlow, E.; Stellato, F.; Proux, O.; Rossi, G.; Exley, C.; Morante, S., X-Ray absorption spectroscopy measurements of Cu-ProIAPP complexes at physiological concentrations. *Condens. Matter* **2019,** *4* (1).
21. Mijovilovich, A.; Hayashi, H.; Kawamura, N.; Osawa, H.; Bruijnincx, P. C. A.; Gebbink, R. J. M. K.; de Groot, F. M. F.; Weckhuysen, B. M., K ss detected high-resolution XANES of Fe^{II} and Fe^{III} models of the 2-His-1-carboxylate motif: Analysis of the carboxylate binding mode. *Eur. J. Inorg. Chem.* **2012,** (10), 1589-1597.
22. Baumgartner, J.; Morin, G.; Menguy, N.; Gonzalez, T. P.; Widdrat, M.; Cosmidis, J.; Faivre, D., Magnetotactic bacteria form magnetite from a phosphate-rich ferric hydroxide via nanometric ferric (oxyhydr)oxide intermediates. *Proc. Natl. Acad. Sci. U.S.A.* **2013,** *110* (37), 14883-14888.
23. Coutaud, M.; Meheut, M.; Glatzel, P.; Pokrovski, G. S.; Viers, J.; Rols, J. L.; Pokrovsky, O. S., Small changes in Cu redox state and speciation generate large isotope fractionation during adsorption and incorporation of Cu by a phototrophic biofilm. *Geochim. Cosmochim. Acta* **2018,** *220*, 1-18.
24. Blazevic, A.; Orlowska, E.; Kandioller, W.; Jirsa, F.; Keppler, B. K.; Tafili-Kryeziu, M.; Linert, W.; Krachler, R. F.; Krachler, R.; Rompel, A., Photoreduction of terrigenous Fe-humic substances leads to bioavailable iron in cceans. *Angew. Chem. Int. Ed.* **2016,** *55* (22), 6417-6422.
25. Lafuerza, S.; García, J.; Subías, G.; Blasco, J.; Glatzel, P., High-resolution Mn K-edge X-ray emission and absorption spectroscopy study of the electronic and local structure of the three different phases in $Nd_{0.5}Sr_{0.5}MnO_3$. *Phys. Rev. B* **2016,** *93* (20), 205108.
26. Calvo, C., The Crystal Structure of α-$Zn_3(PO_4)_2$. *Can. J. Chem.* **1965,** *43* (2), 436-445.
27. Ishioka, T.; Murata, A.; Kitagawa, Y.; Nakamura, K. T., Zinc(II) acetate dihydrate. *Acta Crystallogr., Sect. C* **1997,** *53*, 1029-1031.
28. Skinner, B. J., Unit-Cell Edges of Natural and Synthetic Sphalerites. *Am. Mineral.* **1961,** *46* (11-2), 1399-1411.
29. Zhang, R. H.; Hong, Q. M.; Yang, J. M.; Zhang, H. L.; Blackburnb, G. M.; Zhou, Z. H., Syntheses, spectroscopies and structures of zinc complexes with malate. *Inorg. Chim. Acta* **2009,** *362* (8), 2643-2649.
30. Dadlani, A.; Acharya, S.; Trejo, O.; Nordlund, D.; Peron, M.; Razavi, J.; Berto, F.; Prinz, F. B.; Torgersen, J., Revealing the bonding environment of Zn in ALD Zn(O,S) buffer layers through X-ray absorption spectroscopy. *ACS Appl. Mater. Interfaces* **2017,** *9* (45), 39105-39109.
31. Glatzel, P.; Smolentsev, G.; Bunker, G., The electronic structure in 3d transition metal complexes: Can we measure oxidation states? *J. Phys.: Conf. Ser.* **2009,** *190*, 012046.
32. Waychunas, G. A.; Fuller, C. C.; Davis, J. A.; Rehr, J. J., Surface complexation and precipitate geometry for aqueous Zn(II) sorption on ferrihydrite: II. XANES analysis and simulation. *Geochim. Cosmochim. Acta* **2003,** *67* (5), 1031-1043.
33. Rose, J.; Moulin, I.; Masion, A.; Bertsch, P. M.; Wiesner, M. R.; Bottero, J. Y.; Mosnier, F.; Haehnel, C., X-ray absorption spectroscopy study of immobilization processes for heavy metals in calcium silicate hydrates. 2. Zinc. *Langmuir* **2001,** *17* (12), 3658-3665.
34. Tang, Y. Z.; Chappell, H. F.; Dove, M. T.; Reeder, R. J.; Lee, Y. J., Zinc incorporation into hydroxylapatite. *Biomaterials* **2009,** *30* (15), 2864-2872.
35. Salt, D. E.; Prince, R. C.; Baker, A. J. M.; Raskin, I.; Pickering, I. J., Zinc ligands in the metal hyperaccumulator *Thlaspi caerulescens* as determined using X-ray absorption spectroscopy. *Environ. Sci. Technol.* **1999,** *33* (5), 713-717.

36. Krizek, B. A.; Merkle, D. L.; Berg, J. M., Ligand variation and metal-ion binding-specificity in zinc finger peptides. *Inorg. Chem.* **1993,** *32* (6), 937-940.
37. Krizek, B. A.; Amann, B. T.; Kilfoil, V. J.; Merkle, D. L.; Berg, J. M., A consensus zinc finger peptide - design, high-affinity metal-binding, a pH-dependent structure, and a His to Cys Sequence Variant. *J. Am. Chem. Soc.* **1991,** *113* (12), 4518-4523.
38. García Ruiz, J. Local geometry by XANES and RXS. In *Multiple Scattering Theory for Spectroscopies*, ed. no. 1; Sébilleau, D.; Hatada, K.; Ebert, H., Eds.; Springer International Publishing, 2018; Vol. 204. pp 345-350.
39. Guine, V.; Spadini, L.; Sarret, G.; Muris, M.; Delolme, C.; Gaudet, J. P.; Martins, J. M. F., Zinc sorption to three gram-negative bacteria: Combined titration, modeling, and EXAFS study. *Environ. Sci. Technol.* **2006,** *40* (6), 1806-1813.
40. Webb, S. M.; Gaillard, J. F.; Jackson, B. E.; Stahl, D. A., An EXAFS study of zinc coordination in microbial cells. *J. Synchrotron Radiat.* **2001,** *8*, 943-945.
41. Sarret, G.; Manceau, A.; Spadini, L.; Roux, J. C.; Hazemann, J. L.; Soldo, Y.; Eybert-Berard, L.; Menthonnex, J. J., Structural determination of Zn and Pb binding sites in *Penicillium chrysogenum* cell walls by EXAFS spectroscopy. *Environ. Sci. Technol.* **1998,** *32* (11), 1648-1655.
42. Karlsson, T.; Skyllberg, U., Complexation of zinc in organic soils - EXAFS evidence for sulfur associations. *Environ. Sci. Technol.* **2007,** *41* (1), 119-124.
43. Karlin, S.; Zhu, Z. Y., Classification of mononuclear zinc metal sites in protein structures. *Proc. Natl. Acad. Sci. U.S.A.* **1997,** *94* (26), 14231-14236.
44. Ha, J.; Gelabert, A.; Spormann, A. M.; Brown, G. E., Role of extracellular polymeric substances in metal ion complexation on *Shewanella oneidensis*: Batch uptake, thermodynamic modeling, ATR-FTIR, and EXAFS study. *Geochim. Cosmochim. Acta* **2010,** *74* (1), 1-15.
45. Tan, I. S.; Ramamurthi, K. S., Spore formation in *Bacillus subtilis*. *Environ. Microbiol. Rep.* **2014,** *6* (3), 212-225.
46. Laity, J. H.; Lee, B. M.; Wright, P. E., Zinc finger proteins: New insights into structural and functional diversity. *Curr. Opin. Struct. Biol.* **2001,** *11* (1), 39-46.
47. Kramerschnabel, U.; Linder, P. W., Complexation of zinc(II) and calcium(II) ions with organic monophosphate esters. *J. Coord. Chem.* **1990,** *22* (2), 139-143.
48. Binder, H.; Arnold, K.; Ulrich, A. S.; Zschornig, O., Interaction of Zn^{2+} with phospholipid membranes. *Biophys. Chem.* **2001,** *90* (1), 57-74.
49. Sigel, H.; Griesser, R., Nucleoside 5 '-triphosphates: self-association, acid-base, and metal ion-binding properties in solution. *Chem. Soc. Rev.* **2005,** *34* (10), 875-900.
50. Toner, B.; Manceau, A.; Marcus, M. A.; Millet, D. B.; Sposito, G., Zinc sorption by a bacterial biofilm. *Environ. Sci. Technol.* **2005,** *39* (21), 8288-8294.
51. Finney, L. A.; O'Halloran, T. V., Transition metal speciation in the cell: Insights from the chemistry of metal ion receptors. *Science* **2003,** *300* (5621), 931-936.
52. Capdevila, D. A.; Wang, J. F.; Giedroc, D. P., Bacterial strategies to maintain zinc metallostasis at the host-pathogen interface. *J. Biol. Chem.* **2016,** *291* (40), 20858-20868.
53. Beveridge, T. J.; Murray, R. G. E., Uptake and retention of metals by cell-walls of *Bacillus-subtilis*. *J. Bacteriol.* **1976,** *127* (3), 1502-1518.
54. Legros, S.; Levard, C.; Marcato-Romain, C. E.; Guiresse, M.; Doelsch, E., Anaerobic Digestion Alters Copper and Zinc Speciation. *Environ. Sci. Technol.* **2017,** *51* (18), 10326-10334.
55. Ravel, B.; Newville, M., Athena, Artemis, Hephaestus: Data analysis for X-ray absorption spectroscopy using IFEFFIT. *J. Synchrotron Radiat.* **2005,** *12*, 537-541.